Indian Journal of Engineering & Materials Sciences
Vol. 27, June 2020, pp. 665-669

Corrosion behaviour of dissimilar TIG welded austenitic stainless steel AISI 304 and martensitic stainless steel AISI 420

Abhishek Ghosh* & Pradip Kumar Pal
Mechanical Engineering Department, Jadavpur University, Kolkata 700032, India

Received:29 September 2016 ; Accepted:08 November 2018

Welded joints of dissimilar metals are often required in nuclear and chemical industries. Among the various types of material combinations, welded joint of austenitic stainless steel and martensitic stainless steel is one good option. Due to differences in mechanical, metallurgical and corrosion properties between the two dissimilar materials, selections of suitable welding parameters, filler materials, shielding gas mixture etc. are extremely important in order to avoid drastic thermal gradient, hence significant welding distortions. In the present work, defect free TIG welding of dissimilar materials AISI 304 and AISI 420 has been made successfully. Quality of the welded joint has been judged through tensile test, microstructural investigation, micro-hardness measurement, SEM fractography and XRD analysis. Corrosion behaviour of the welded joint at different concentrations of NaCl has been measured through potentio-dynamic polarization. Weldment shows passivity at different solutions.

Keywords: AISI 304 austenitic stainless steel, AISI 420 martensitic stainless steel, Dissimilar TIG welding, Weld quality

1 Introduction

Dissimilar martensitic/austenitic welded joints are used in the nuclear and thermal power plants[1]. Martensitic stainless steels are used (specially in water-evaporators and steam headers) due to their good thermal conductivity, low thermal expansion coefficient, good thermal fatigue resistance and lower cost; on the other hand, austenitic stainless steels are used (specially in superheaters and reheaters) for their good corrosion resistance, high creep strength and high temperature stability of the microstructure during service[1, 2].

Martensitic stainless steels are Fe-C-Cr alloy having bct crystal structure[3]. They are ferro-magnetic, hard, brittle and heat-treatable. Austenitic stainless steels are interstitial solid solution of carbon with fcc crystal structure[4]. They are non-magnetic, non-heat treatable, tough and ductile. Huge differences in mechanical and metallurgical properties between these two types of stainless steels have complicated the tasks of engineers to weld them.

Kacar and Baylan[5] welded X5CrNi18-10 austenitic and X20CrMo13 martensitic stainless steel of 10 mm thickness by MMAW process using both E2209-17 duplex and E308L-16 austenitic filler wire. Preheating was done at 200°C temperature. Falat *et al.*[6] TIG welded martensitic T91 and austenitic TP316H tubes of 5.6 mm wall thickness using Ni-based filler metal Thermanit Nicro 82. AISI 420 martensitic and AISI 304 austenitic stainless steel were successfully welded by Halvaee *et al.*[7] by Nd: YAG laser welding. Berretta *et al.*[8] used resistance upset welding. Yang *et al.*[1, 9] TIG welded i) T92/HR3C and ii) T92/S304H martensitic-austenitic combinations of stainless steels using AWS ERNiCr-3 (Inconel) filler metals. Bhaduri *et al.*[2] TIG welded 403 martensitic and 304 L(N) austenitic stainless steel using ER308L, ER309L and ERNiCr-3 filler wires. Srinivasan[10] experimented electrochemical corrosion behavior of TIG welded AISI 316 austenitic stainless steel and AISI 410 martensitic stainless steel dissimilar weld joint.

Though very few works regarding dissimilar welding of AISI 420 martensitic and AISI 304 austenitic stainless steel material combinations have been reported in literature but performance of TIG welding is not reported at all. Corrosion behavior of Weld and HAZ zone is not reported also though study of corrosion behavior of weldment is extremely important if the joint is used in power plants.

In the present work, corrosion behaviour of the dissimilar welded joint has been studied at different concentrations of NaCl and H_2SO_4.

2 Experimental Procedure

2 mm thick sheets of martensitic stainless steel AISI 420 and austenitic stainless steel AISI 304

*Corresponding author (E-mail: a.ghosh865@gmail.com)

Table 1 — Chemical composition of base materials.

	C (%)	Cr (%)	Mn (%)	Si (%)	S (%)	P (%)	Cu (%)	Ni (%)	Mo (%)	Fe (%)
AISI 420	0.19	12.68	0.45	0.28	0.007	0.032	-	0.17	-	86.2%
AISI 304	0.08	18.45	1.52	0.61	0.02	0.035	-	8.92	0.05	70.3%
ER 309L	0.03	24.0	1.8	0.5	-	-	0.2	13.1	0.3	60.07%

Table 2 — Mechanical properties of base materials.

	Yield Strength (MPa) at 0.2% offset	UTS (MPa)	Percentage elongation (%)	Hardness (HRB)
AISI 420	363.02	536.91	13.14	82.3
AISI 304	321.56	631.26	61.80	89.7

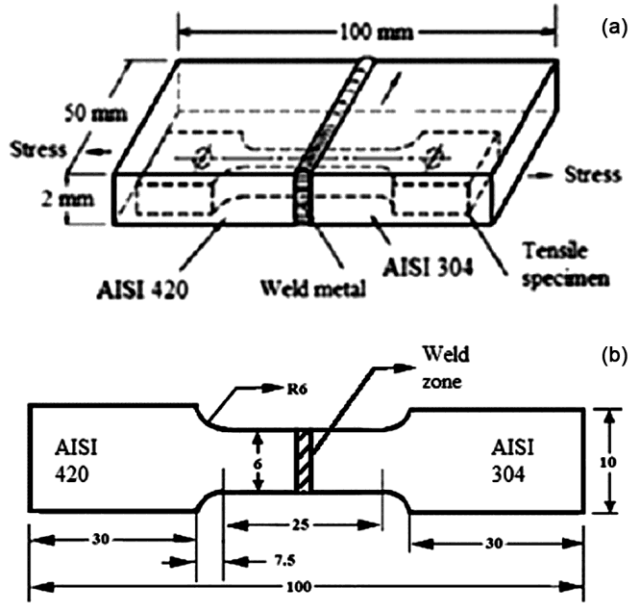

Fig. 1 — Tensile test specimen (a) Cutting out a tensile test specimen and (b) ASTM E8 sub-size specimen.

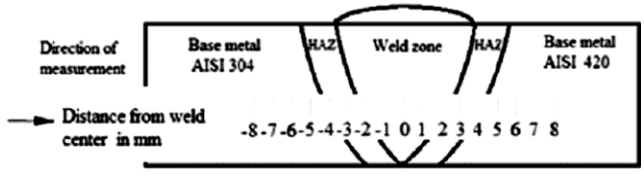

Fig. 2 — Location of hardness measurement at different zones.

(50 mm length × 50 mm width) have been used for square butt welding in the present investigation. Welding has been completed in one pass. Four such specimens (specimen 1-4) have been prepared for study.

Chemical compositions of the base materials and filler metal have been shown in Table 1. Mechanical properties of base metals have been tested and shown in Table 2. Welding has been done using ER 309L filler wire of 1.6 mm diameter. M_s temperature of AISI 420 material has been calculated using Andrews's[11] formula and it is 288.5°C. Pre-heating at 250°C

Table 3 — Result of tensile tests.

Sp. no	UTS (MPa)	Elongation (%)	Position of failure
1	520	33.2	AISI 420 base metal
2	480	33.8	Weld zone
3	530	34.2	AISI 420 base metal
4	550.25	36.05	AISI 420 base metal

temperature has been given to both base metals to avoid drastic thermal gradient during welding followed by high residual stress at as-welded condition. 99% pure Argon shielding has been ensured during welding at 12 lit/min flow rate. Open circuit voltage, welding current and welding speed have been maintained at 11 V, 80 A and 1.1 mm/sec, respectively. 2 % thoriated tungsten TIG welding electrode of 1.6 mm diameter has been used. Above mentioned levels have been selected after several trial runs. ASTM E8 standard has been followed to prepare tensile test specimen (Fig. 1). Tensile test specimens have been cut by a wire-cut EDM. Tensile tests have been carried out by Instron universal testing machine. Leica metallurgical microscope (model no. DMLM/11888605) has been used for microstructural study. After welding, samples have been cut transversely from the welds and then mechanically grounded (300-2000 mesh using grinding paper), polished (1µm diamond paste) and finally etched by aqua regia (HCl: HNO_3 = 3:1). LECO LM 248AT micro-hardness tester has been used to measure hardness profile of weldment (Fig. 2). Fracture analysis of fractured tensile test specimen has been carried out using SEM (Jeol JSM-5510). X-ray diffraction analysis of the welded joint has been done by Rigaku-Ultima IV machine. Corrosion tests have been performed using Gamry potentiostat.

3 Results and Discussion

3.1 Tensile Test

Tensile test specimens have been prepared from welded samples. Results of tensile tests have been tabulated in Table 3.

Most of the welded samples (Except sample no. 2) have retained their strength close to the strength of AISI 420 base metal at as-welded condition, fracture being taken place from AISI 420 base metal zone. This can be attributed to thermal, metallurgical, heating and cooling behaviour of the molten materials of two different kinds. Further, the welding parameters do influence the mechanical properties.

More investigation is being planned in this respect to analyze the results more critically. Stress-strain curves of two base metals and one welded joint (specimen 4) have been shown in Fig. 3a. Fractured surface of the tensile test specimen have been analysed by SEM fractography test (Fig. 3b), brittle fracture has been observed.

3.2 Hardness Measurement

Non-uniform hardness profiles have been observed for the weldment at as-welded conditions (Fig. 4), higher hardness at HAZ compared to base metals and weld zone has been observed. This may be due to the fact that HAZ remains in as-quenched condition after welding. More is discussed in section 3.3.

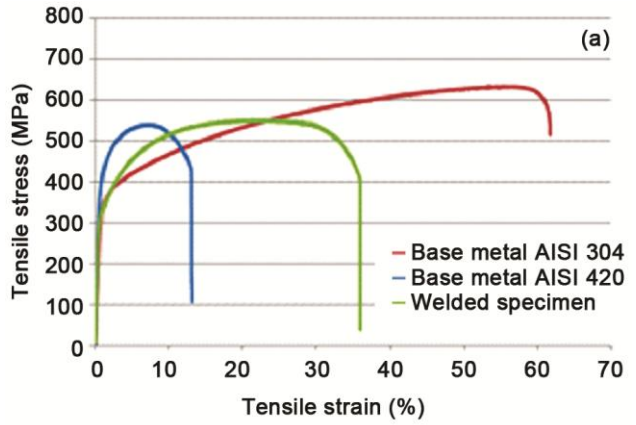

Fig. 3 — Tensile test of weldment (a) Stress-strain curve of base materials and welded specimen and (b) Fractured surface analysis.

3.3 Microstructural Investigation

Microstructures of welded joint (weld zone and HAZ) at different regions have been shown in Fig. 5

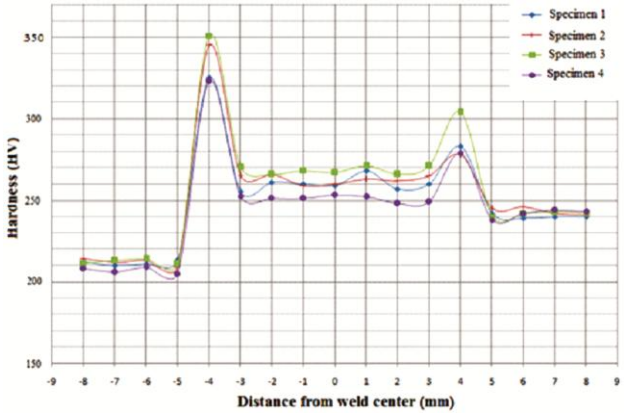

Fig. 4 — Hardness of weldment.

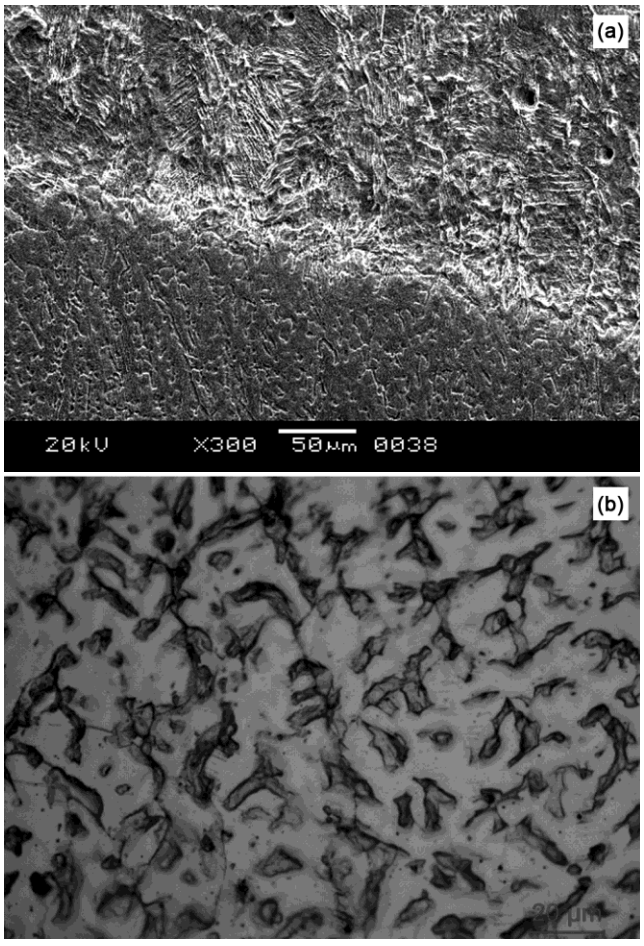

Fig. 5 — Microstructure of weldment (Specimen 1) (a) SEM image (Weld-HAZ zone) and (b) Optical microscope image (Weld zone).

(a-b). Columnar dendritic grain growth has been observed in weld zone. Grain growth has been observed in HAZ. No carbide precipitation has been identified at HAZ.

Microstructure of the fusion zone consists of austenite matrix with both skeletal and acicular ferrite; ferrite is observed in austenite grain boundaries. The HAZ region adjacent to the martensitic stainless steel base material, consists of non-tempered and tempered martensites. Columnar grain growth to the direction of martensitic base metal has been observed as heat transformation coefficient of the martensitic stainless steel base metal is higher than that of austenitic base metal. Higher hardness in HAZ region of both side of fusion zone is attributed to the formation of acicular martensitic structure. Presence of ferrite phase reduces the hardness in the fusion zone.

3.4 XRD Analysis

Phases present in the weld-HAZ composite zone (containing HAZ of both sides of weld zone and weld zone) have been found through X-ray diffraction analysis (Fig. 6). Magnetite (M) is found to be dominant phase along with very complex compounds chromite, maghemite etc. Data have been collected in the range $20°\leq 2\theta \leq 100°$. XRD analysis establishes the presence of δ-ferrite. Complex chromites found in this are not expected.

3.5 Corrosion Test

In 0.5 M sulphuric acid solution the corrosion potentials of the sample is found to be close to −531 mV versus SCE and with addition of chloride (0.1 M NaCl + 0.5M H_2SO_4 solution), the potential has been observed as −678 mV versus SCE. With addition of 0.1 M and 0.5 M chloride in 1 M sulphuric acid solution the corrosion potentials of the weldment has been observed to shift towards the nobler side, with the values measured as -384 mV versus SCE and -380 mV versus SCE, respectively. But high corrosion rate was observed in 0.5 M NaCl + 1 M H_2SO_4 solution as the respective corrosion current is found to be very high (387.1×10^{-6} A cm^{-2}).

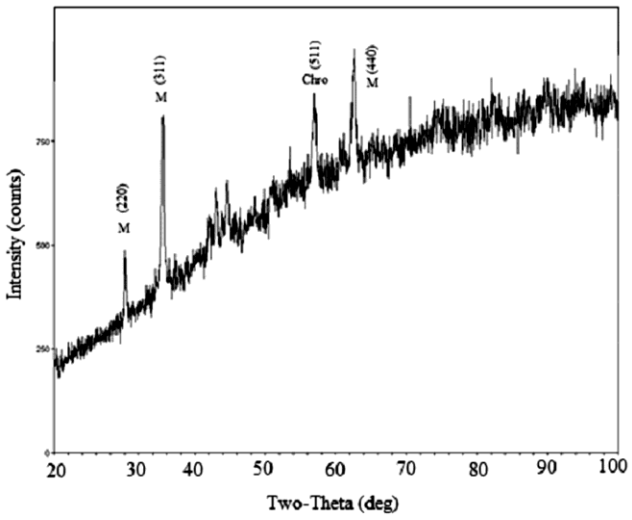

Fig. 6 — XRD pattern of welded joint.

Corrosion behaviours of the welded joint at different concentrations of NaCl and H_2SO_4 (1% NaCl, 3.5% NaCl, 1M H_2SO_4, 0.1 M NaCl + 0.5 M H_2SO_4, 0.1 M NaCl + 1 M H_2SO_4, 0.5 M NaCl + 1 M H_2SO_4) have been studied.

Corrosion samples (containing HAZ and weld zone) exhibit passivity in corrosion tests at room temperature (30°C). Corrosion current densities have been determined from polarization curves by Tafel extrapolation method. Corrosion parameters including corrosion current density (i_{corr}) and electrode potential (E_c) have been enlisted in Table 4. Polarization curves at different solutions have been shown in Fig. 7 (a-f). Significant increase in corrosion current density has been observed in 0.5 M NaCl + 1 M H_2SO_4 solution compared to other solutions. SEM image of the corroded sample has been shown in Fig. 8.

In 1% NaCl solution the weldment has registered a corrosion potential of −500 mV vs. SCE with a corrosion current density of 7.72×10^{-6} A cm^{-2}. The sample is found to have active corrosion potentials and the corrosion potential (−528 mV vs. SCE) is found to drift towards the active side with increase in chloride (3.5% NaCl) concentration in the test electrolyte.

These observations reaffirm that the general corrosion behaviour of the dis-similar GTA weldment is not influenced by the microstructural transformations and the weldment is safe from the perspective of galvanic corrosion. Presence of un-tempered martensitic structure with small amounts of ferrite in the weld/HAZ zone does not adversely influence the corrosion behaviour.

Table 4 — Corrosion parameters.

Solution	Icorr (A/cm^2)	E corr (mV)
1% NaCl	7.72×10^{-6}	-500
3.5% NaCl	17×10^{-6}	-528
0.5 M H_2SO_4	14×10^{-6}	-531
0.1 M NaCl + 0.5 M H_2SO_4	26.72×10^{-6}	-678
0.1 M NaCl + 1 M H_2SO_4	30×10^{-6}	-384
0.5 M NaCl + 1 M H_2SO_4	387.1×10^{-6}	-380

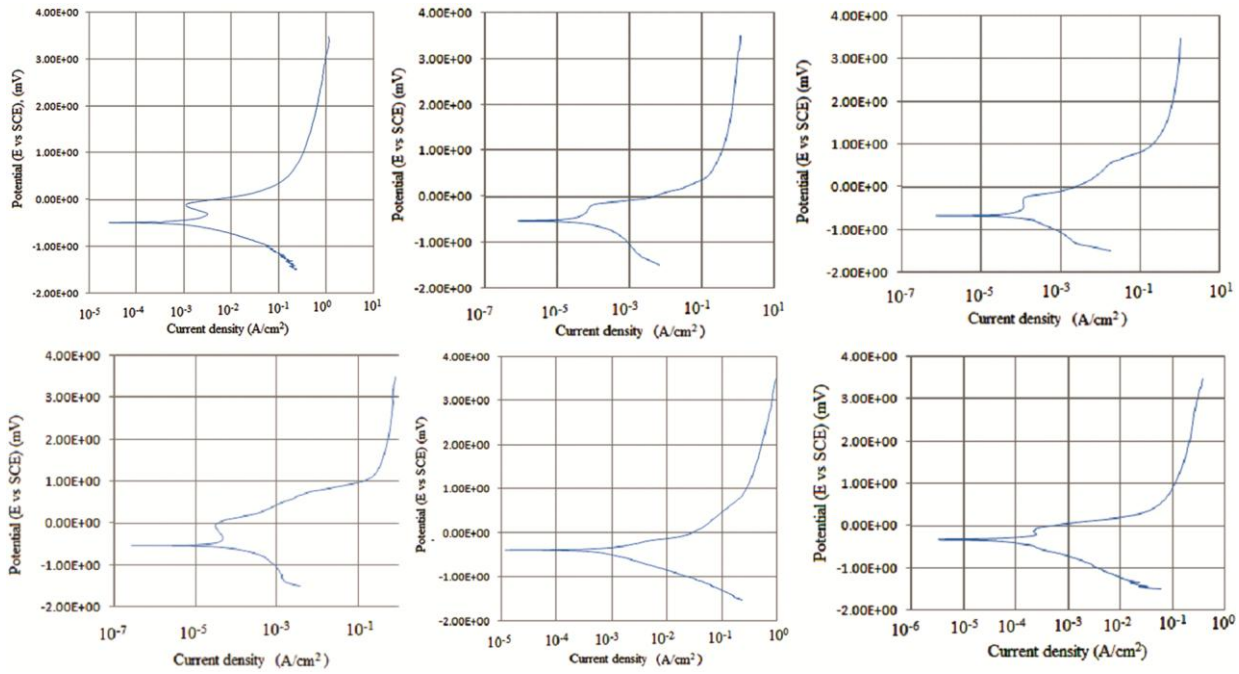

Fig. 7 — Polarization curves at different solutions (a) 1% NaCl , (b) 3.5% NaCl, (c) 0.5 M H_2SO_4, (d) 0.1 M NaCl + 0.5 M H_2SO_4, (e) 0.1 M NaCl + 1 M H_2SO_4 and (f) 0.5 M NaCl + 1 M H_2SO_4.

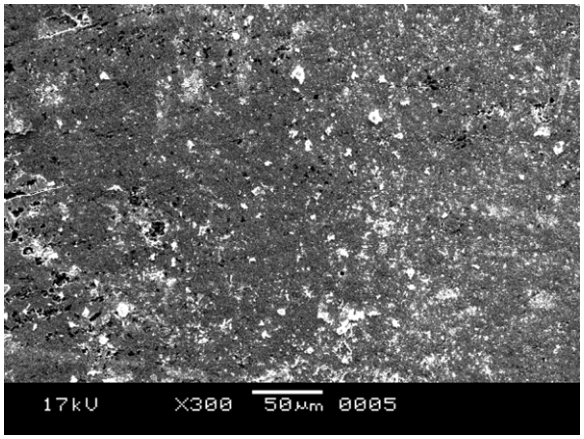

Fig. 8 — SEM image of corroded sample.

4 Conclusions

On the basis of the experimental work done and interpretation of the results, the following conclusions have been drawn for dissimilar TIG welding of AISI 304 austenitic stainless steel and AISI 420 martensitic stainless steel:

(i) AISI 304 austenitic stainless steel can be welded satisfactorily to AISI 420 martensitic stainless steel using ER 309L electrode using preheat at 250°C temperature.

(ii) Dissimilar weldment exhibits an acceptable joint strength. In fracture analysis, brittle fracture has been has been observed. HAZ remains in as-quenched condition after welding. Significantly higher hardness has been observed in HAZ compared to base materials and weld zone.

(iii) Weld-HAZ composite zone exhibits passivity at corrosion tests. Corrosion resistance of the welded joint is found to be satisfactory.

References

1 Cao J, Gong Y, Yang Z, Luo X, Gu F& Hu Z, *Int J Pressure Vessels Piping*, 88 (2011) 94.

2 Das C R, Bhaduri A K, Srinivasan G, Shankar V & Mathew S, *J Mater Process Technol*, 209 (2009) 1428.

3 Isfahany A N, Saghafian H & Borhani G, *J Alloys Compounds*, 509 (2011) 3931.

4 Cisquini P, Ramos S V, Viana P R P, CunhaLins V F, Franco Jr A R, Ribeiro A & Vieira E A, *J Mater Res Technol*, 8 (2019) 1897.

5 Kacar R & Baylan O, *Mater Des*, 25 (2004) 317.

6 Falat L, Svobod M, Výrostková A, Petryshynets I & Sopko M, *Mater Character*, 72 (2012) 15.

7 Sharifitabar M & Halvaee A, *Mater Des*, 31 (2010) 3044.

8 Berretta J R, Rossi W, Neves M D M, Almeida I A & Junior N D V, *Opt Lasers Eng*, 45 (2007) 960.

9 Cao J, Gong Y, Zhu K, Yang Z, Luo X & Gu F, *Mater Des*, 32 (2011) 2763.

10 Srinivasan P B & Kumar M P S, *Mater Chem Phys*, 115 (2009) 179.

11 Andrews K W, *J Iron Steel Inst*, 203 (1965) 721.